Eur. Phys. J. A **8**, 103–114 (2000)

THE EUROPEAN PHYSICAL JOURNAL A

Analytical calculation of fusion cross-sections

R. Arora[a], R.K. Puri, and R.K. Gupta

Center of Advanced Study in Physics, Panjab University, Chandigarh-160014, India

Received: 24 February 1999 / Revised version: 21 September 1999
Communicated by P. Schuck

Abstract. We analyse the fusion cross-sections, calculated by using two different analytical parameterisations and compare them with the experimental data. Both the parameterisations are based on ion-ion potentials calculated within the framework of Skyrme energy density formalism. In the first case, the ion-ion potential (including the spin-density term) was parameterised and then, by adding the Coulomb potential, one could compute the fusion barrier analytically. In the second case, the calculated fusion barrier heights and positions were parameterised directly. Both of these (previously) reported parameterisations are used here to calculate the fusion barriers and fusion excitation functions for more than 50 reactions belonging to the *s-d* and *f*-shell nuclei. A detailed comparison of these parametrisations with the experimental and several other theoretical results shows that both of these parameterisations are able to reproduce the experimental data equally well. As the (second) direct parameterisation depends only on the charges and masses of colliding nuclei, it is very useful for predicting/ understanding the fusion process in low energy heavy-ion reactions.

PACS. 25.70.-z Low and intermediate energy heavy-ion reactions – 25.70.Jj Fusion and fusion-fission reactions – 24.10.-i Nuclear-reaction models and methods – 25.60.Pj Fusion reactions

1 Introduction

One of the primary goals of low energy heavy-ion physics is to understand the fusion of colliding nuclei and related phenomena [1]. Depending on the incident energy and angular momentum, the collision of two nuclei can lead to complete (or partial) fusion, multifragmentation, subthreshold particle production, etc. [2]. The fusion of nuclei is a low density phenomenon and several calculations have been made in recent years to search for the nuclear structure effects and enhancement in fusion cross-sections at sub-barrier energies [1,3,4]. During the last more than three decades, huge experimental data on fusion cross-sections and excitation functions has accumulated [5-20]. Most of the experiments performed at low energies involve a variety of targets and projectiles. Some experiments are performed for the symmetric (or nearly symmetric) colliding nuclei (like Ca+Ca, O+O, etc.) whereas others involve very asymmetric colliding nuclei (like $^{16}O/^{27}O + ^{70-76}Ge, ^{16}O + ^{147-149}Sm, ^{16-18}O + ^{208}Pb$, etc.) [5-20].

On the other hand, the many theoretical attempts involve several different models/ theories [21-31]. Here one starts from a microscopic Hamiltonian and calculates the nucleus-nucleus interaction potential. The Hamiltonian used in these calculations contains all the necessary quantum features. The Hamiltonian density functionals used in these approaches contain mainly the ones due to Skyrme Energy Density Functional (EDF) of Vautherin and Brink [32], its modification by Brack et al. [24] where the spin-orbit energy density is written in a semi-classical way, and the Brueckner Energy density functional [33]. Most of the calculations of ion-ion potentials are done either in the spirit of the folding model [1,22] or in the spirit of energy density model [21,23,28]. The energy density model involves the densities of both the composite and individual nuclei whereas the same in folding model are only for the individual nuclei. Recently, the Skyrme EDF has been used within the concept of proximity theorem where the spin-orbit density part of the Hamiltonian is also included [22,25,28]. The spin-orbit density part of the Hamiltonian was neglected in all previous studies. Recently, two of us had generalised the spin-orbit density part of the Hamiltonian to the case of unclosed shell nuclei which opened up a new possibility in the study of low energy fusion excitation functions [28]. The effect of the spin-orbit density part (for spin-unsaturated nuclei) towards fusion cross-section can be quite appreciable [22,25,30]. Apart from this, a recent study has also suggested a linear enhancement of the fusion cross-sections with the addition of neutrons to colliding N=Z nuclei [4]. Furthermore, as the fusion process is a low density phenomenon, it occurs at the surface of the colliding nuclei. In other words, it occurs at the surface of the interaction potential and hence the inner part of the ion-ion potential is not relevant for our present study. This means that a study of fusion excitation functions

[a] Also at: Khalsa College for Women, Civil Lines, Ludhiana (Panjab), India

indicates the validity of any particular approach at the surface region only.

Several attempts have been made in the past to parameterize the ion-ion potentials in terms of some known quantities like the masses and charges of colliding nuclei. One of the basic ideas in parameterizing the ion-ion potential (in terms of masses and charges of colliding nuclei) is that these quantities are known a priori in any experiment. Therefore, such a parameterized form of the ion-ion potential can be of great importance if the accuracy of the results is not destroyed. Two different parameterizations have been proposed for the Skyrme energy density formalism [21,29–31]:

(i) In the first method, several authors have parameterized the ion-ion potential and then, by adding the Coulomb potential, one could compute the fusion barriers and hence the cross-sections [21,23,29,31]. All these attempts use only the spin-independent part of the ion-ion potential. As the spin-dependent term of the Hamiltonian is neglected, these parameterizations are done in the spirit of proximity theorem by parameterizing the universal function. For the first time a complete parameterization of the ion-ion potential was presented by two of us which also included the spin-orbit density term of the Hamiltonian [31]. The parameterization of the spin-orbit density part of the potential involves different shells and, therefore, does not allow to intermix the different shells. In other words, this analytical parameterization of the ion-ion potential is done for nuclei belonging to the same shell [31]. It may be mentioned here that in the self consistent semi-classical (SCSC) approach of Brack et al. [24], as was used by Li et al. [25] to compute the nucleus-nucleus interaction potential, the spin-orbit effects are independent of the shell. Thus, if one parameterizes the calculated nucleus-nucleus potential within the SCSC approach, one could extract a complete analytical parameterization of the nucleus-nucleus potential (including the spin-orbit part) which would be independent of the shell structure of the colliding nuclei [25].

(ii) In the second method, some calculations are reported where the fusion barriers (their positions and heights) are parameterized directly [21,30]. In such an attempt, we first calculated the fusion barriers and positions for a large number of reactions and then parameterized them in terms of the charges and masses of the colliding nuclei. This parameterization needed a least square fit of the third order [30].

Unfortunately, while reporting the above mentioned two parameterizations, nearly no effort was made to compare the results of these parameterizations with the experimental fusion excitation functions [30,29,31]. Therefore, in order to demonstrate the utility of these powerful parameterizations, we present here a detailed comparison of the results of these two parameterizations with the exact calculations and also compare them with the experimental data. Also, a detailed comparison is made with other theoretical results.

In the following, we first discuss briefly the energy density formalism and then give the details of our (already reported) parameterizations in Sect. 2. Our results are presented in Sect. 3. Finally, we summarize the results in Sect. 4.

2 The skyrme energy density formalism and the analytical methods

We shall first discuss the theoretical framework of the Skyrme Energy Density Formalism [SEDF] [32] which is used here to parameterize the ion-ion interaction potential and the fusion barriers. In SEDF, the interaction potential is calculated as:

$$V_N(R) = E(R) - E(\infty) = \int [H(\rho,\tau,\mathbf{J}) - H_1(\rho_1,\tau_1,\mathbf{J_1}) - H_2(\rho_2,\tau_2,\mathbf{J_2})]\, d\mathbf{r}, \quad (1)$$

with ρ_i ($=\rho_\pi+\rho_\nu$), τ_i ($=\tau_\pi+\tau_\nu$) and $\mathbf{J}_i$ ($=\mathbf{J}_\pi+\mathbf{J}_\nu$), being the nucleon density, kinetic energy density and spin-orbit density, respectively, for each nucleus ($i = 1,2$). Here π and ν refers to proton and neutron, respectively. Then, using sudden approximation, $\rho = \rho_1+\rho_2$, $\tau = \tau_1+\tau_2$ and $\mathbf{J} = \mathbf{J}_1+\mathbf{J}_2$. This approximation is valid if the time of collision is much shorter than the relaxation time. If the collision time is much longer than the relaxation time, the density of the overlapping region will rearrange itself into a state with lowest energy. As our present interest is to look for the fusion probabilities, the sudden approximation is a good approximation.

The Hamiltonian density $H(\rho,\tau,\mathbf{J})$ in (1) stands for the energy density functional, which is given by [32] as

$$\begin{aligned} H(\rho,\tau,\mathbf{J}) &= \\ &= \frac{\hbar^2}{2m}\tau + \frac{1}{2}t_0[(1+\frac{1}{2}x_0)\rho^2 - (x_0+\frac{1}{2})(\rho_\pi^2+\rho_\nu^2)] \\ &+ \frac{1}{4}(t_1+t_2)\rho\tau + \frac{1}{8}(t_2-t_1)(\rho_\pi\tau_\pi+\rho_\nu\tau_\nu) \\ &+ \frac{1}{16}(t_2-3t_1)\rho\nabla^2\rho + \frac{1}{32}(3t_1+t_2)(\rho_\pi\nabla^2\rho_\pi+\rho_\nu\nabla^2\rho_\nu) \\ &+ \frac{1}{4}t_3\rho_\pi\rho_\nu\rho - \frac{1}{2}W_0(\rho\nabla\cdot\mathbf{J}+\rho_\pi\nabla\cdot\mathbf{J}_\pi+\rho_\nu\nabla\cdot\mathbf{J}_\nu). \end{aligned} \quad (2)$$

Here, the six parameters t_0, x_0, t_1, t_2, t_3 and W_0 are fitted by various authors to reproduce the various ground state properties of some nuclei. These different parameterizations are dubbed as Skyrme Forces S, SI, SII, SIII, etc. We shall use here the Skyrme force SIII whose parameters are: $t_0 = -1128.75 MeV fm^3$, $t_1 = 395 MeV fm^5$, $t_2 = -95 MeV fm^5$, $t_3 = 14000 MeV fm^6$, $W_0 = 120 MeV fm^5$ and $x_0 = 0.45$. A careful look at (2) shows that the Hamiltonian $H(\rho,\tau,\mathbf{J})$ can be divided into two parts: (i) the spin-independent part, and (ii) the spin-dependent part [28], as

$$\begin{aligned} V_N(R) &= \int [H(\rho) - (H_1(\rho_1)+H_2(\rho_2))]\, d\mathbf{r} \\ &\quad + \int [H(\rho,\mathbf{J}) - (H_1(\rho_1,\mathbf{J}_1)+H_2(\rho_2,\mathbf{J}_2))]\, d\mathbf{r} \\ &= V_P(R) + V_J(R). \end{aligned} \quad (3)$$

Naturally, the spin-independent part of the Hamiltonian $H(\rho)$ (the τ can also be written in terms of ρ [28], as discussed below) depends on the density of the colliding nuclei only and, therefore, is a smooth varying function of the nuclear mass. This part of the potential is calculated by using the proximity concept of Blocki et.al [27]. The use of proximity concept restricts the above formulation to medium and heavy nuclei. The second part of the Hamiltonian H(**J**) depends on the spin-orbit density **J** which is a function of the radial wave functions and hence the shell structure of the nucleus. In other words, we cannot use the proximity concept for calculating the spin-orbit density part of the potential.

For the nucleon-density ρ in (2), we use the Fermi type of density distribution:

$$\rho_i(Z_i) = \rho_{oi}\left[1+\exp\left(\frac{Z_i - R_{oi}}{a_i}\right)\right]^{-1};\ -\infty \le Z \le \infty, \quad (4)$$

with $Z_2 = R - Z_1$ for the motion in Z-direction of a plane. Here $R_{oi}(= C_i$, the central radii for Fermi density distribution) and a_i are, respectively, the half density radii and surface thickness parameters whose variations with mass number A of the nucleus are studied in [28]. In a recent calculation [28], we have shown that for the spin density part of the potential, our use of above Fermi density distribution yields nearly the same result as for the microscopic shell model density i.e. the density calculated within the shell model description of using the harmonic oscillator wave functions for the radial part.

The kinetic energy density τ used in (2) is taken from Thomas Fermi approximation corrected for the additional surface effects due to von Weizsacker:

$$\tau = \frac{3}{5}\left[\frac{3}{2}\pi^2\right]^{2/3}\rho^{5/3} + \lambda\frac{(\nabla\rho)^2}{\rho}. \quad (5)$$

The value of the constant λ has been a point of controversy in the literature and a value between 1/36 and 9/36 is suggested. Note that by using the above approximation for τ, a large part of the exchange effects can be taken into account. In the present calculations, we put $\lambda = 0$ for SIII force but take $\lambda = 1/36$ for the SII force used for comparisons. Alternatively, one could use for τ the extended Thomas-Fermi approximation of Brack et al. [24, 25].

For more details, the reader is referred to [28]. In the following, we discussed our (previously) reported analytical formulations that are based on SEDF.

2.1 Analytical formulation of the ion-ion interaction potential [AFIP]

In an attempt to parameterize the ion-ion interaction potential, the spin-independent part $V_P(R)$ and the spin-dependent part $V_J(R)$ of the potential were parameterized separately [29,31]. The idea behind this separate parameterization was that $V_P(R)$ depends only on the geometry of the system whereas $V_J(R)$ also depends on its shell structure. In the spirit of proximity potential, the spin-independent part of the ion-ion potential can be parameterized as

$$V_P(R) = 2\pi\bar{R}\Phi(s) \quad (6)$$

with $\bar{R} = \frac{C_1C_2}{C_1+C_2}$, $C_i = R_i - \frac{1}{R_i}$, R_i (i=1 or 2) being radius of target and projectile, respectively. The universal function $\Phi(s)$ was parameterized as [29,31]:

$$\Phi(s) = \begin{cases} -\Phi_0\ \exp\left[-0.3325(s-s_0)^2\right], & \text{for } s \ge s_0, \\ -\Phi_0 + 1.90(s-s_0)^2, & \text{for } s \le s_0 \end{cases} \quad (7)$$

with Φ_0=2.27 (MeV/fm) and s_0=0.2 fm. Here s $(= R - C_1 - C_2)$ is the surface distance between two nuclei. Note that the universal function $\Phi(s)$ does not depend on the nature of the colliding nuclei and hence is an universal function. Once the nuclear radii are calculated, one can calculate the spin-independent part of the ion-ion potential $V_P(R)$ analytically.

The analytical formulation of the spin-dependent part $V_J(R)$ of the potential is more complicated [31]. This is due to fact that $V_J(R)$ is a function of the radial wave functions which depend strongly on the shell structure of a nucleus. It is worth to remind here that the radial wave functions vary smoothly within a shell. In other words, the analytical parameterization of the spin-dependent part of the ion-ion potential is possible only within a shell. Therefore, the AFIP is limited to those reactions where colliding nuclei belong to same shell. This should not affect our interest if we are studying the *sd* or *0f* shell nuclei.

The spin-dependent part of the ion-ion potential $V_J(R)$ was parameterized as [31]:

$$V_J(R) = \begin{cases} V_{JB}\ \exp\left[\zeta\left(\frac{R-R_{JB}}{R_{JL}-R_{JB}}\right)^{\frac{5}{3}}\right], \ for\ R \ge R_{JB} \\ V_{JB} - V_{JB}\left(\frac{R-R_{JB}}{R_{J0}-R_{JB}}\right)^2, \quad for\ R \le R_{JB} \end{cases} \quad (8)$$

Here $\zeta = ln[(0.003)/V_{JB}]$. The maxima of the spin-density potential (V_{JB}) was represented by:

$$V_{JB} = \alpha_i P_s, \quad (9)$$

P_s being the "Particle-strength" of a reaction, and is given by:

$$P_s = \sum_{i=1}^{2}\left[\sum_\alpha \frac{(2j_\alpha+1)}{4\pi}[j_\alpha(j_\alpha+1) - l_\alpha(l_\alpha+1) - \frac{3}{4}] \pm \frac{n_v}{4\pi}[j(j+1) - l(l+1) - \frac{3}{4}]\right] \quad (10)$$

Here n_v is the number of valence particles (or holes) outside (or inside) a closed core and i shows the index of colliding nuclei. The values of the constants α_i in (9) depend on the shell and are summarized in Table 1. All other quantities (i.e. R_{JB}, R_{J0}, and R_{JL}) are parameterized in terms of the masses of colliding nuclei, as

$$R_i = \beta_i + \gamma_i(A_1A_2), \qquad (i = JB, J0, JL). \quad (11)$$

Table 1. The values of constants α, β and γ in (7) and (9) for colliding nuclei belonging to different shells

Colliding nuclei (shells)	V_{JB} α	R_{JB} $\beta_{JB}\gamma_{JB}$	R_{J0} $\beta_{J0}\gamma_{J0}$	R_{JL} $\beta_{JL}\gamma_{JL}$
0d+0d	1.5750	$4.74\ 1.07 \times 10^{-3}$	$3.68\ 8.87 \times 10^{-4}$	$9.62\ 2.26 \times 10^{-3}$
0f+0f	1.1333	$6.19\ 3.22 \times 10^{-4}$	$4.77\ 2.88 \times 10^{-4}$	$10.63\ 8.29 \times 10^{-4}$

The constants α_i, β_i and γ_i for the colliding nuclei belonging to different shells i.e. (sd+sd) and (0f+0f) shells are also listed in Table 1. Note that the above parameterization involves only the charges and masses of colliding nuclei.

Once $V_P(R)$ and $V_J(R)$ are calculated by using (6)–(11), the total interaction potential $V_T(R)$ can be calculated by adding the Coulomb interaction term:

$$V_T(R) = V_P(R) + V_J(R) + \frac{Z_1 Z_2 e^2}{R}. \quad (12)$$

The barrier position R_B and height V_B are then determined by the conditions

$$\frac{dV_T(R)}{dR}|_{R=R_B} = 0 \quad \text{and} \quad \frac{d^2V_T(R)}{dR^2}|_{R=R_B} \leq 0. \quad (13)$$

Using the parameterized form of the ion-ion potential, one can calculate the fusion barrier positions and heights and hence the cross-sections analytically. The advantage of AFIP is that it gives a possibility to compute the total ion-ion potential as well as the barriers analytically. On the other hand, it is limited to those reactions where colliding nuclei belong to the same shell.

2.2 The direct parameterization of fusion barriers [DPFB]

In [30], we had proposed a direct parameterization of the fusion barriers, calculated within the energy density formalism. Several tens of reactions were calculated by using the SEDF and then a simple parameterization was given for the fusion barrier positions and heights. The barriers were parameterized in terms of the masses and charges of target and projectile nuclei. These calculated interaction barriers reproduced the empirical fusion barrier heights and positions within a few percent of accuracy. A similar attempt was also made by Ngŏ et al. [21], but their parameterization led to larger deviations.

In this method, the parameterization of the fusion barrier height is governed by the fact that Coulomb interaction contributes largely toward fusion barrier. Therefore, the fusion barrier height V_B was parameterized in terms of $\Gamma = \frac{Z_1 Z_2}{A_1^{1/3}+A_2^{1/3}}$ [30]:

$$V_B = (0.845 \pm 0.020)\Gamma + (1.30 \mp 0.25) \times 10^{-3}\Gamma. \quad (14)$$

In the same way, the barrier position R_B was parameterized in terms of the product of masses of the two colliding nuclei $A_P = (A_1 A_2)$:

$$R_B = 7.359 + 3.076 \times 10^{-3} A_P - 1.182 \times 10^{-6} A_P^2 + 1.567 \times 10^{-10} A_P^3. \quad (15)$$

Thus, the direct parameterization [DPFB] depends on $Z_1, Z_2,\ A_1, A_2$ only. This means that once the reaction partners are known, one can compute the fusion barrier heights and positions directly. Note that in this parameterization we have no information about the ion-ion potential $V(R)$; the only available information is about the fusion barrier height and position. The major advantage, however, is that this parameterization is not restricted to any shell. Therefore, it is an universal parameterization. On the other hand, the disadvantage of this parameterization is that the fusion barrier positions were parameterized with the help of a least square fit which means that the microscopic structure is missing in this parameterization.

If one looks at (14) and (15), and Figs. 5 and 6 of [30], one finds that the present DPFB is valid only for the light and medium mass colliding nuclei. If one goes to very heavy nuclei, say, with $Z_1 \cdot Z_2 \geq 1000$, (14) and (15) will yield very large values of V_B and R_B. Therefore, our present description of DPFB should be applied only to the light and medium mass colliding nuclei. A new complete parameterization, which is also valid for heavy systems, is in progress [34].

A comparison of two different analytical methods (AFIP and DPFB) with large number of experimental data will give an unique possibility to test the validity of these parameterizations. In view of the limitation of AFIP, however, we restrict ourselves to the colliding nuclei belonging to the same shell.

3 Results and discussion

In the following, we compare the fusion barriers and cross-sections calculated by using the energy density formalism for Skyrme force SIII within the above mentioned two analytical parameterizations, the AFIP and DPFB. An attempt will also be made to compare these two calculations with other theoretical model predictions and the experimental data.

First of all, we shall demonstrate the performance of our analytical expressions for the nucleus-nucleus potentials by comparing them with several other theoretical model predictions. In Fig. 1, we compare the spin-orbit density independent ($\mathbf{J} = 0$) part of the potential, calculated by using the AFIP with the self-consistent semi-

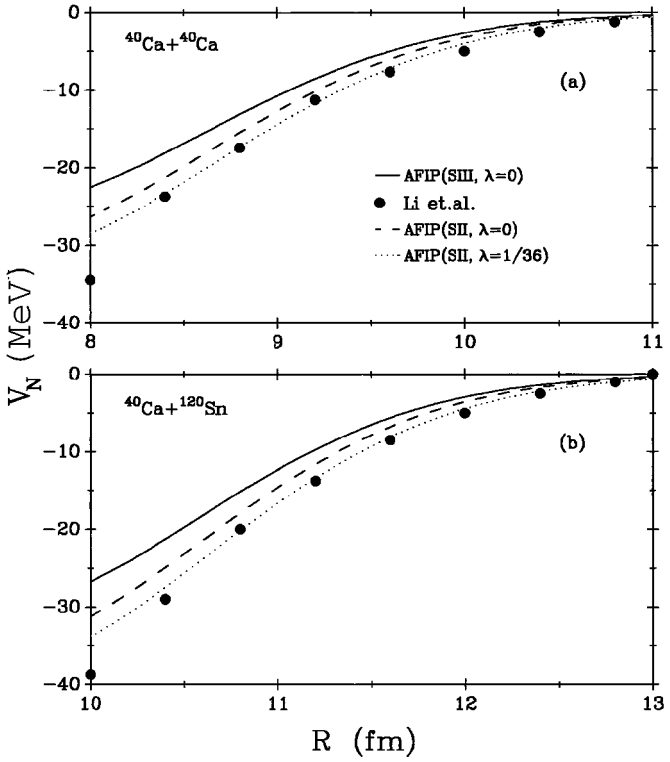

Fig. 1. The nucleus-nucleus potential calculated by using AFIP(SIII, $\lambda = 0$), AFIP(SII, $\lambda = 0$), AFIP(SII,$\lambda = 1/36$), compared with that of Li et.al [25] calculations. The results with AFIP(SIII), AFIP(SII) exclude the spin-orbit part of the potential. The curves of Li at.al. are extracted from [25]. Part (a) is for $^{40}Ca + ^{40}\,Ca$ reaction whereas part (b) is for $^{40}Ca + ^{120}\,Sn$ reaction

classical (SCSC) theory of Li et.al [25]. Only the relevant surface part of the potential is shown. Figures 1(a) and 1(b) are, respectively, for the collisions $^{40}Ca + ^{40}\,Ca$ and $^{40}Ca + ^{120}\,Sn$. In order to see the effect of using different Skyrme forces and also of different λ-values in Thomas-Fermi approximation for kinetic energy density (5), we have also displayed the results of the parameterized potentials calculated by using the Skyrme force SII (with and without $\lambda = 1/36$). These parameterizations read as [30]:

$$V_P(R) = 2\pi\bar{R} \begin{cases} -2.64 \ \exp\left[-0.3250(s-0.2)^2\right], & \text{for s } \geq 0.2, \\ -2.64 + 2.15(s-0.2)^2, & \text{for } s \leq 0.2 \end{cases} \quad (16)$$

for $\lambda = 0$, and

$$V_P(R) = 2\pi\bar{R} \begin{cases} -2.84 \ \exp\left[-0.3045(s-0.2)^2\right], & \text{for s } \geq 0.2, \\ -2.84 + 1.895(s-0.2)^2, & \text{for } s \leq 0.2 \end{cases} \quad (17)$$

for $\lambda = 1/36$, denoted as AFIP(SII, $\lambda = 0$) and AFIP(SII, $\lambda = 1/36$), respectively. We notice in Fig. 1 that the AFIP(SII,$\lambda = 0$) is reasonably close to SCSC calculations of Li et.al [25], but if one adds a contribution due to non-zero value of λ (see AFIP(SII, $\lambda = 1/36$), the two match almost exactly. Note that the SCSC calculations are done by using an extended Thomas Fermi approximation for kinetic energy density τ which also includes $\lambda = 1/36$ contribution. In a similar way, if one includes the non-zero value of λ in AFIP for SIII force, one should expect a better agreement with the SCSC calculations of Li et al. [25].

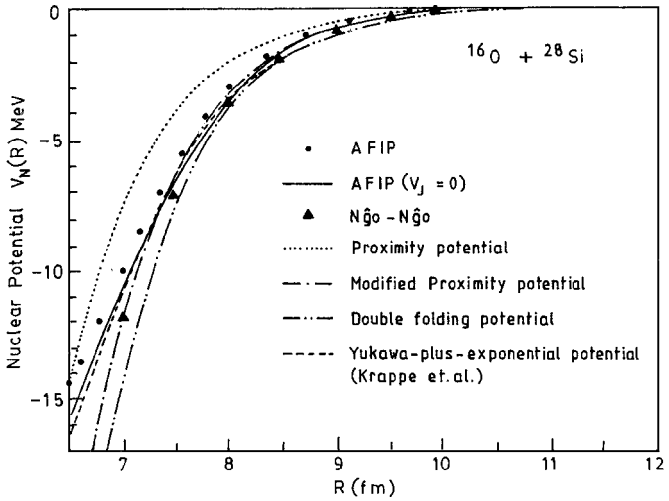

Fig. 2. Same as for Fig. 1, but for $^{16}O + ^{28}\,Si$ and for using AFIP, AFIP(V_J=0), double folding potential, proximity potential, Yukawa-plus-Exponential potential of Krappe at.el. modified proximity potential and Ngŏ-Ngŏ parameterization extracted from [1]. The AFIP calculations are for SIII, $\lambda = 0$ case

Figure 2 depicts a further comparison of our calculated AFIP(SIII) potential with other theoretical model potentials, for the reaction of $^{16}O + ^{28}$Si. This includes the proximity potential, its modified version, the double folding potential and the Yukawa-plus-exponential potential. All these potential are taken from [1]. The cases of both with and without spin-orbit contribution $V_J(R)$ are plotted for AFIP(SIII). Interesting enough, all these models, though vary strongly in their assumptions, give nearly the same attraction at surface. For the proximity potential, its modified version matches better with all other potentials. The standard proximity potential yields very weak attraction at the surface. Also, the agreement of AFIP(SIII) with other models is shown improved once its spin-dependent part is removed. This is understandable because all other potentials also exclude this dependence.

In Figs. 3 and 4, we display for the barrier heights V_B and positions R_B, the percentage differences between the calculations for AFIP and DPFB, respectively, and the ones calculated by using (i) standard proximity potential (ii) Yukawa-plus-Exponential potential (iii) Brueckner EDF potential due to Ngŏ-Ngŏ and (iv) the double folding potential. All these values are taken from the compilation of Vaz et al. [1]. From Figs. 3 and 4, we find that our AFIP and DPFB reproduce the barrier heights and posi-

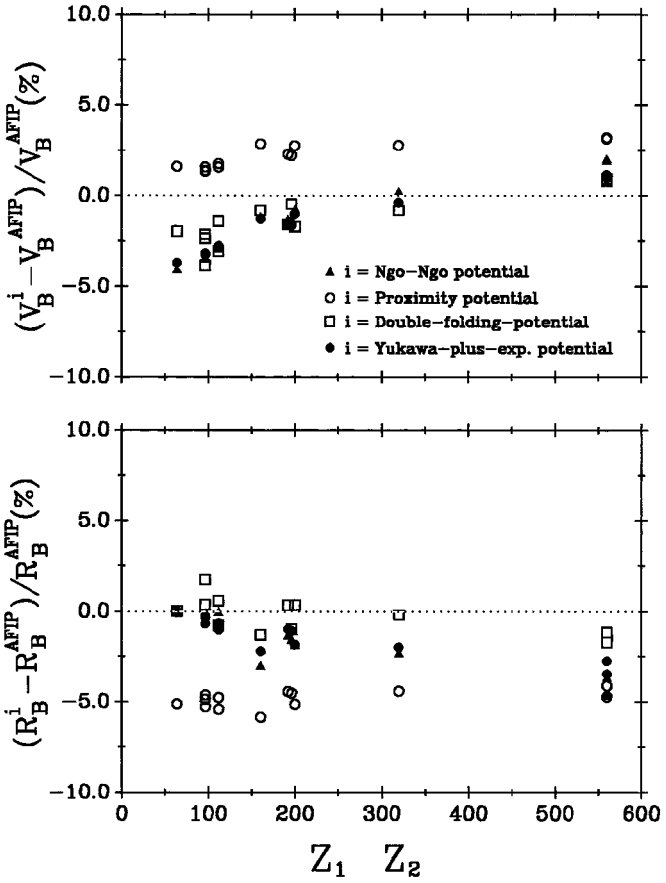

Fig. 3. The normalized differences between the calculations made with AFIP and various other theoretical models. These values are taken from [1]. The upper pannel is for V_B whereas the lower pannel represents R_B

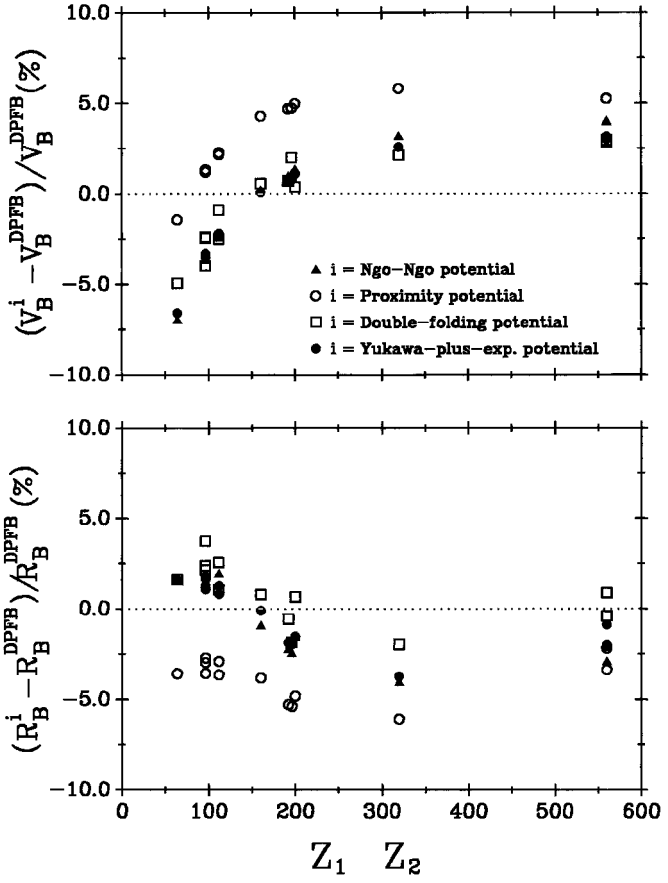

Fig. 4. Same as for Fig. 3, but for the differences between DPFB and other theoretical models

tions within $\approx 5\%$ of the other theoretical model predictions. A comparison of our parametrized fusion barriers (AFIP and DPFB) with the empirical data is also made later in Table 2 and Fig. 7.

Figure 5 shows a plot of the fusion excitation functions, calculated by using the sharp cut off model:

$$\sigma_{fus} = \pi R_B^2 [1 - \frac{V_B}{E_{c.m.}}]. \tag{18}$$

The calculations are made for the reaction of $^{16}O + ^{16}O$ and $^{16}O + ^{40}Ca$, using various models, namely AFIP, DPFB, proximity potential, Yukawa-plus-exponential potential Ngŏ-Ngŏ potential and the double folding potential. Note that both AFIP and DPFB are for SIII force and the two reactions are cases of spin-saturated nuclei, i.e. the spin-dependent part of the potential is zero. We find that all theoretical potentials yield nearly the same result, the standard proximity potential yielding somewhat lower fusion cross-sections for $^{16}O + ^{40}Ca$ reaction. Hence, it is clear that our both analytical parameterizations AFIP and DPFB are able to reproduce the other theoretical model predictions very closely.

Next, we shall attempt to compare our results with the available experimental data. We study the fusion of more than 50 reactions which involve the symmetric as well as asymmetric reaction partners, with asymmetry parameter $\eta(= \frac{(A_1 - A_2)}{A_1 + A_2}) = 0$ to 0.43. In Table 2, we list the fusion barrier heights and positions, calculated by using the exact energy density formalism (exact EDF) and the two analytical formulae of interaction potential [AFIP] and the direct parameterization of fusion barrier [DPFB]. For comparisons, we also list the empirical calculations which are fitted to experimental data. Here we display only those reactions where experimental data on (V_B, R_B) are available. We see that in most of the cases, all the three calculations i.e. the exact EDF, the AFIP and the DPFB, reproduce the experimental data quite nicely. This shows the validity of above parameterizations.

In order to quantify the results of Table 2, we first plot in Fig. 6 the results of our AFIP and DPFB calculations normalized to the exact EDF results. The upper and lower pannels of the figure are for V_B and R_B, respectively. The plotted quantities give the percentage differences in V_B and R_B calculated by using exact EDF and the AFIP/DPFB. We notice that in all cases, the parameterized form of the interaction potential or fusion barriers reproduces the exact EDF results within about $\pm 5\%$. Note that the barrier heights for heavy colliding nuclei with $Z_1 Z_2 \geq 200$ can be reproduced rather more accurately, thereby stressing the validity of the analytical

Table 2. Fusion barrier heights and positions calculated with exact EDF and the two analytically parametrized model AFIP and DPFB. The empirical data is also displayed for comparisons. The empirical data marked with * are used for further comparisons in Fig. 6. Note that in our earlier use of AFIP [29] $s = R - R_1 - R_2$, whereas the same here is defined more consistently as $s = R - C_1 - C_2$. The earlier definition yields higher fusion cross-sections

System	exact EDF		AFIP		DPFB		Empirical Values	
	V_B (MeV)	R_B (fm)	V_B (MeV)	R_B (fm)	V_B (MeV)	R_B (fm)	V_B (MeV)	R_B (fm)
$^{16}O + ^{16}O$	10.97	7.90	10.61	8.20	10.94	8.07	11.00	7.60
							11.20±0.6	7.60±0.4
							10.91	8.20*
$^{16}O + ^{20}Ne$	12.81	8.37	13.05	8.35	13.22	8.23	13.40	8.22
$^{16}O + ^{24}Mg$	15.07	8.43	15.38	8.52	15.42	8.38	15.90±0.9	8.40±0.4
$^{16}O + ^{26}Mg$	14.83	8.64	15.18	8.62	15.20	8.45	16.50±0.9	8.70±0.4
$^{16}O + ^{28}Si$	17.25	8.55	17.65	8.67	17.56	8.51	17.23	7.98
$^{18}O + ^{28}Si$	16.68	8.93	17.34	8.80	17.24	8.63	16.90	8.76
$^{16}O + ^{40}Ca$	23.98	8.94	24.03	9.07	23.71	8.89	23.70±1.0	9.00±0.4
							23.70	9.03*
$^{18}O + ^{24}Mg$	14.55	8.71	15.11	8.65	15.13	8.48	14.90±0.9	7.80±0.3
							14.80	7.82*
$^{20}Ne + ^{20}Ne$	15.18	8.73	15.98	8.50	16.00	8.41	15.20	8.42
$^{20}Ne + ^{40}Ca$	28.64	9.21	29.55	9.17	28.93	9.14	28.60	9.32
$^{24}Mg + ^{24}Mg$	21.19	8.96	22.21	8.80	21.90	8.77	21.53±0.5	8.37±0.2
							22.30±0.4	8.90±0.3*
$^{24}Mg + ^{26}Mg$	20.88	9.07	21.92	8.95	21.60	8.86	20.80±0.5	8.33±0.2
$^{24}Mg + ^{32}S$	27.68	9.09	28.74	9.02	28.08	9.10	28.10±1.6	8.70±0.3
							27.93	9.20*
$^{24}Mg + ^{28}Si$	24.39	8.98	25.51	8.94	25.02	8.94	24.64±0.6	8.11±0.2
$^{26}Mg + ^{32}S$	27.29	9.20	28.38	9.17	27.71	9.19	27.48	9.36
$^{24}Mg + ^{34}S$	27.37	9.29	28.41	9.21	27.77	9.17	27.38	9.40
$^{26}Mg + ^{34}S$	27.00	9.40	28.06	9.31	27.41	9.26	27.11	9.50
$^{28}Si + ^{28}Si$	28.12	9.10	29.33	9.04	28.63	9.12	28.89	8.94*
							28.95±0.7	8.25±0.2
$^{28}Si + ^{30}Si$	27.82	9.26	28.98	9.18	28.28	9.20	29.13	8.86*
							28.28±0.7	8.47±0.2
$^{30}Si + ^{30}Si$	27.54	9.31	28.65	9.32	27.94	9.28	28.54	9.06
$^{32}S + ^{40}Ca$	44.30	9.50	45.37	9.52	44.06	9.69	43.30±4.5	9.00±0.7
$^{40}Ca + ^{40}Ca$	54.26	9.68	55.10	9.78	53.86	9.90	50.60±2.8	9.50±0.5
							55.60±0.8	9.10±0.6*
							52.30±0.5	8.80±0.5
$^{40}Ca + ^{44}Ca$	53.41	9.92	54.27	9.98	52.94	9.97	51.70±1.2	8.50±0.5
$^{40}Ca + ^{48}Ca$	52.60	10.06	53.48	10.16	52.10	10.02	51.30±1.0	7.80±0.3
$^{40}Ca + ^{58}Ni$	73.16	10.02	74.03	10.17	72.57	10.09	73.36	10.20
$^{40}Ca + ^{62}Ni$	72.34	10.19	73.04	10.38	71.63	10.11	72.30	10.35
$^{58}Ni + ^{58}Ni$	99.03	10.26	99.63	10.50	98.90	10.30	97.90	8.30
$^{48}Ti + ^{58}Ni$	78.62	10.25	79.50	10.44	78.11	10.14	78.80	9.80
$^{48}Ti + ^{60}Ni$	78.22	10.39	78.98	10.55	77.61	10.16	77.30	10.00
$^{40}Ca + ^{46}Ti$	58.80	9.84	59.63	9.99	58.22	9.99	58.03	9.92
$^{40}Ca + ^{48}Ti$	58.35	9.91	59.20	10.01	57.76	10.02	58.17	9.97

parameterizations of either interaction potential $V(R)$ or fusion barriers directly. Figure 7 shows the same quantities but with respect to the empirical results, i.e. percentage $\frac{V_B^i - V_B^{emp}}{V_B^{emp}}$ and $\frac{R_B^i - R_B^{emp}}{R_B^{emp}}$. We see that both analytical formulae are able to reproduce the experimental data within a few percent of accuracy. Explicitly, the barrier height are reproduced within almost 5 %, but the barrier positions lie within 10 % of empirical data. The maximum systematic difference occurs only for the light colliding nuclei. From Fig. 7(b), one also notices that in some cases there are huge differences between the calculations using AFIP/DPFB and the experimental data. In this connection, we would like to add here that in most of these cases, either several data are available or the empirical values do not follow the general trends. For example, in the case of $^{58}Ni + ^{58}Ni$ reaction, the empirical fusion barrier position reads as 8.30 fm which is small compared to several cases involving lighter nuclei. Note that in Table 2 and Figures 6 and 7 only those reactions are displayed where

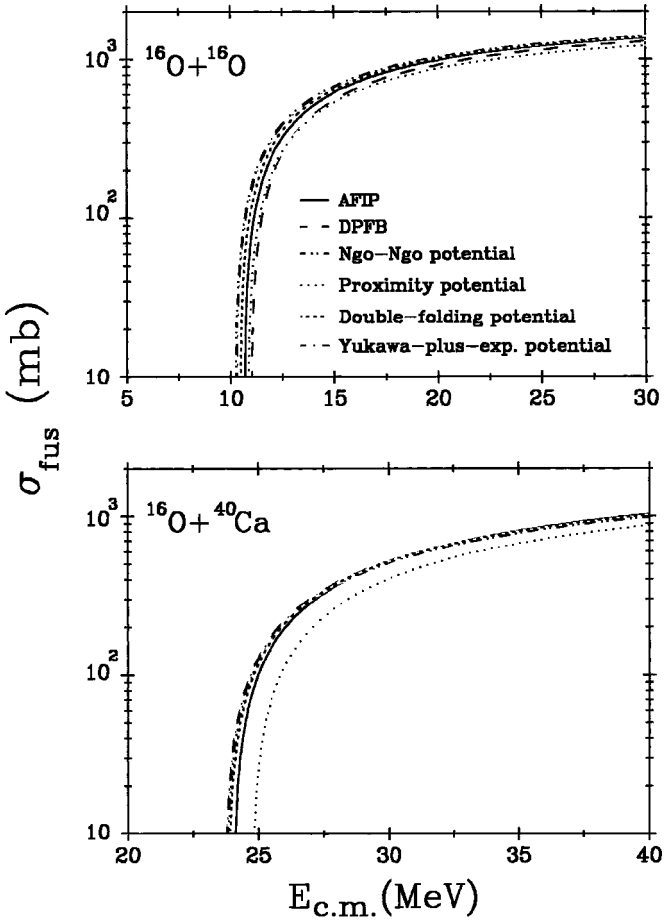

Fig. 5. The fusion excitation functions using AFIP, DPFB and other theoretical models reported in Figs. 3 and 4. Calculations are made for SIII, $\lambda = 0$ case. The upper and lower pannels are, respectively, for $^{16}O +^{16} O$ and $^{16}O +^{40} Ca$ reactions

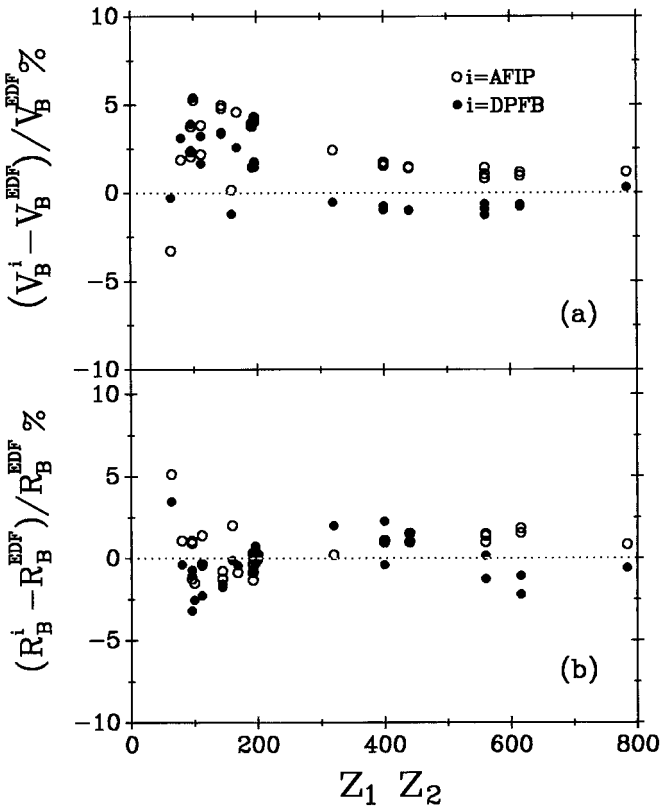

Fig. 6. The normalized differences between the calculations made with AFIP and DPFB and the exact EDF results as a function of the product of charges of two colliding nuclei. The upper and lower parts of the figure are for fusion barrier heights and fusion positions, respectively. The AFIP and DPFB are denoted by solid and open circles, respectively

target and projectile belong to the same shell. This restriction is needed only for AFIP but not for DPFB as this does not depend on the shell structure.

Putting the above results of Figs. 3, 4, and 7 together, we find that all the models, including our own reproduces the empirical barrier heights within $\leq 5\%$ whereas for barrier positions, our analytical model overestimates others by 5%. However, the crucial test of these parameterizations is the calculation of fusion excitation functions. Once the fusion barrier height V_B and position R_B are known, the fusion cross-section can be calculated by using (18). In Figs. 8 and 9, we display the fusion excitation functions for the $^{16-18}O$ induced reactions. Here dashed and solid lines correspond to calculations of AFIP and DPFB, respectively. The experimental data is shown by solid symbols. Specifically, we show the fusion cross-sections for $^{16}O +^{16} O$, $^{16}O +^{20} Ne$, $^{16}O +^{24} Mg$ and $^{16}O +^{26} Mg$ in Fig. 8 and $^{16}O +^{28} Si$, $^{18}O +^{28} Si$, $^{18}O +^{24} Mg$ and $^{16}O +^{40} Ca$ in Fig. 9. First of all, we note that ^{16}O and ^{40}Ca, being closed shell nuclei, do not contribute towards spin-orbit density potential. Therefore, in the reactions of ^{16}O with ^{16}O or ^{40}Ca the only contribution comes from the spin-independent part of the interaction potential. We see that both parameterizations yield nearly the same good result of comparing closely with the experimental data. In some cases, like $^{16}O +^{16} O$, our calculations show only the general trends since different experimental data differ by as much as 200 mb.

Figures 10, 11 and 12 display the parameterized and experimental fusion excitation functions for highly spin-unsaturated reacting partners. Again, in all cases, we see that both AFIP and DPFB are able to reproduce the experimental data equally well. In Fig. 12, we have also shown the dependence of cross-sections on adding neutrons. Starting with $^{28}Si +^{28} Si$ reaction we add 2-neutrons to one or both the reaction partners forming the $^{28}Si +^{30} Si$ and $^{30}Si +^{30} Si$ reactions. We see that the addition of neutrons enhances the fusion cross-section appreciably. A full systematic study of the enhancement in fusion cross-sections with the addition of neutrons is reported in [4].

Figures 13, 14 and 15 deal with fusion excitation functions for still heavier nuclei, like $^{40,44,48}Ca$, $^{46-48}Ti$ and $^{58,60,62}Ni$. Note that ^{40}Ca is a spin-saturated case whereas ^{58}Ni is highly spin-unsaturated. Once again, all experimental fusion excitation functions are reproduced nicely by the simple AFIP and DPFB models.

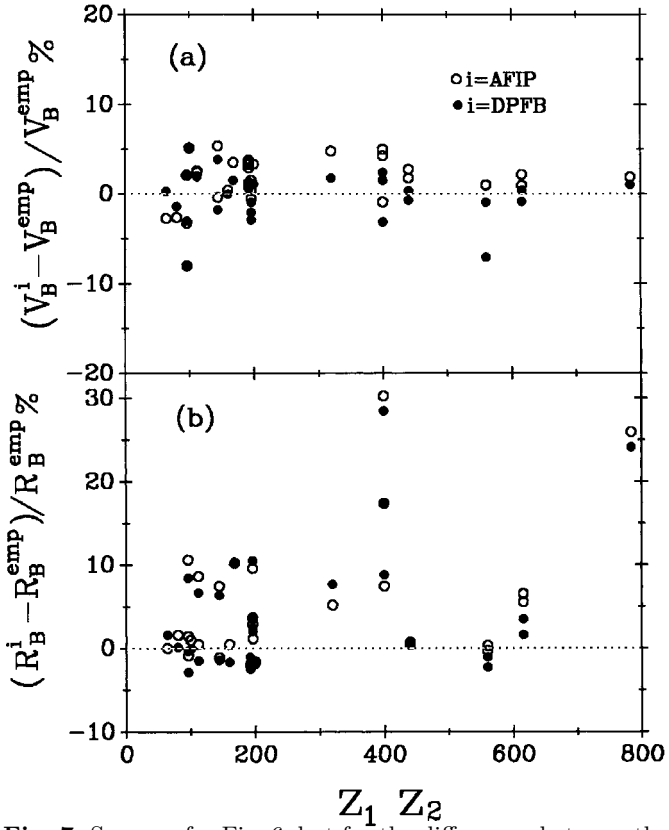

Fig. 7. Same as for Fig. 6, but for the differences between the calculations made with AFIP and DPFB and the empirical values. Note that if there are more than one empirical values available, the one marked with ($\star$) in Table 2 are taken for comparisons

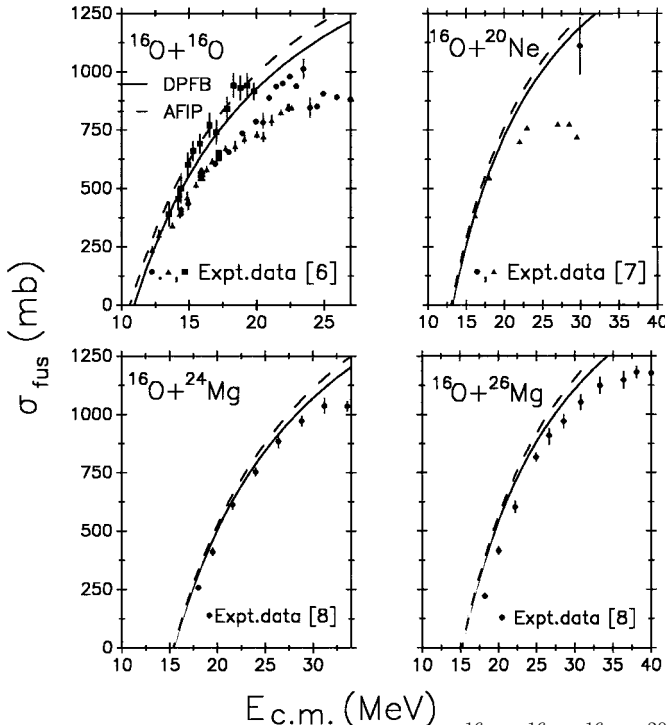

Fig. 8. The fusion excitation functions for $^{16}O+^{16}O$, $^{16}O+^{20}Ne$, $^{16}O+^{24}Mg$ and $^{16}O+^{26}Mg$ reactions. The experimental data is taken from [6-8]

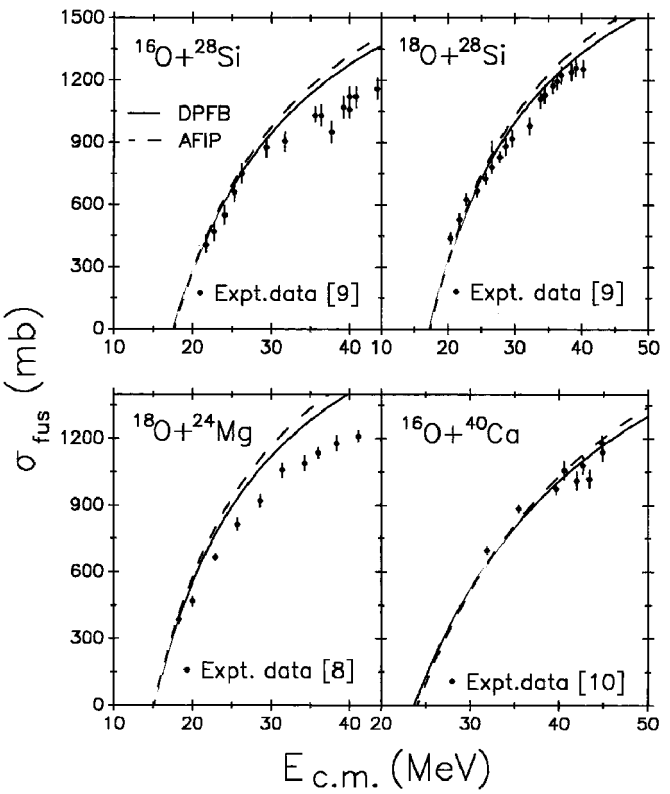

Fig. 9. Same as for Fig. 8, but for $^{16}O+^{28}Si$, $^{18}O+^{28}Si$, $^{16}O+^{24}Mg$ and $^{16}O+^{40}Ca$ reactions. The experimental data is taken from [8-10]

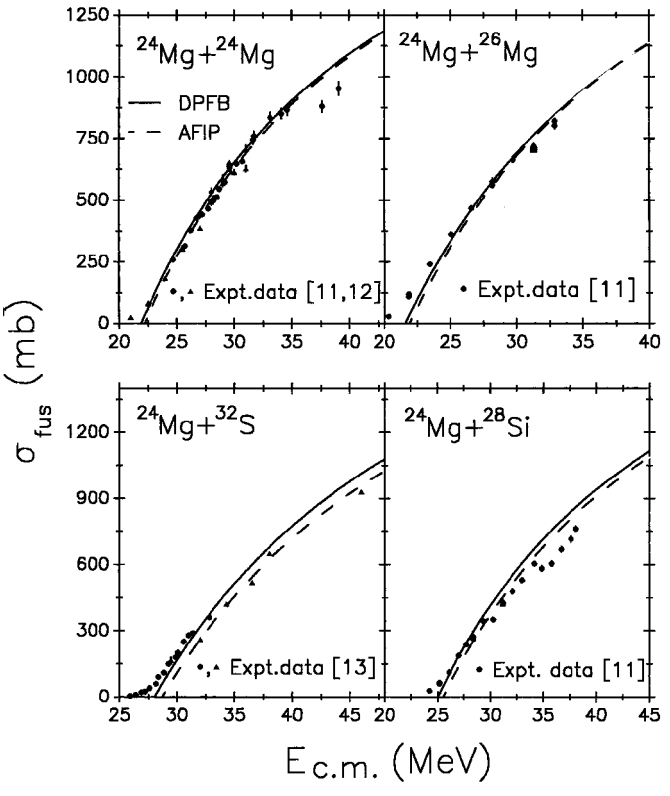

Fig. 10. Same as for Fig. 8, but for $^{24}Mg+^{24}Mg$, $^{24}Mg+^{26}Mg$, $^{24}Mg+^{32}S$ and $^{24}Mg+^{28}Si$ reactions. The experimental data is taken from [11-13]

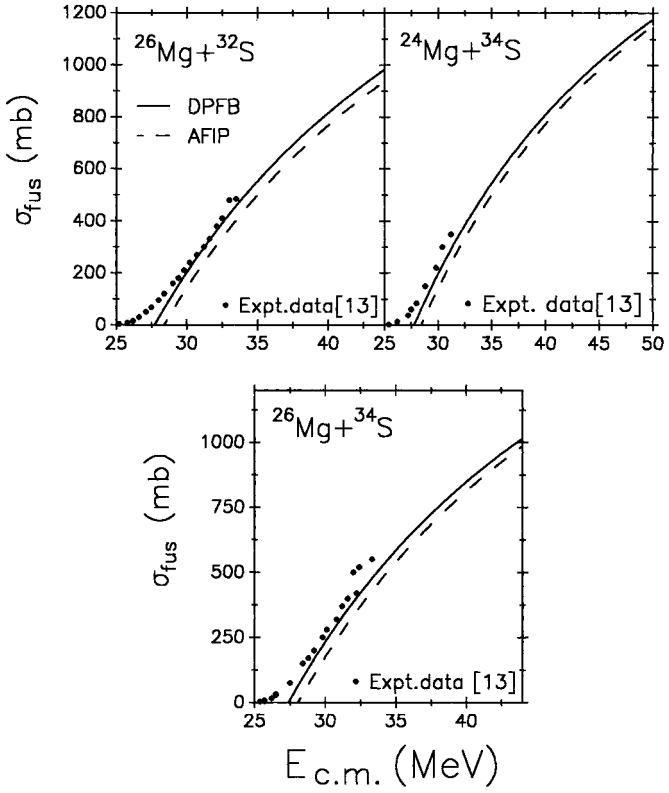

Fig. 11. Same as for Fig. 8, but for $^{26}Mg+^{32}S$, $^{24}Mg+^{34}S$, and $^{26}Mg+^{34}S$

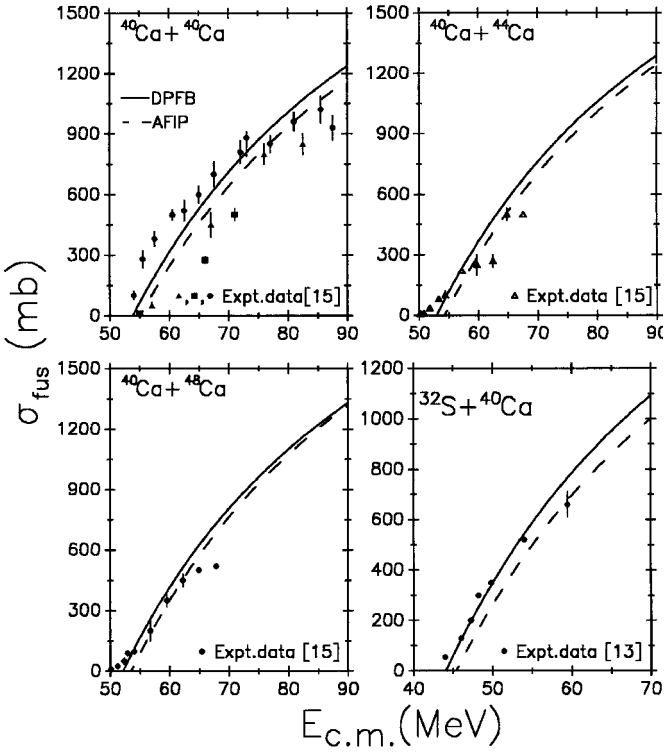

Fig. 13. Same as for Fig. 8, but for $^{40}Ca+^{40}Ca$, $^{40}Ca+^{44}Ca$, $^{40}Ca+^{48}Ca$ and $^{32}S+^{40}Ca$

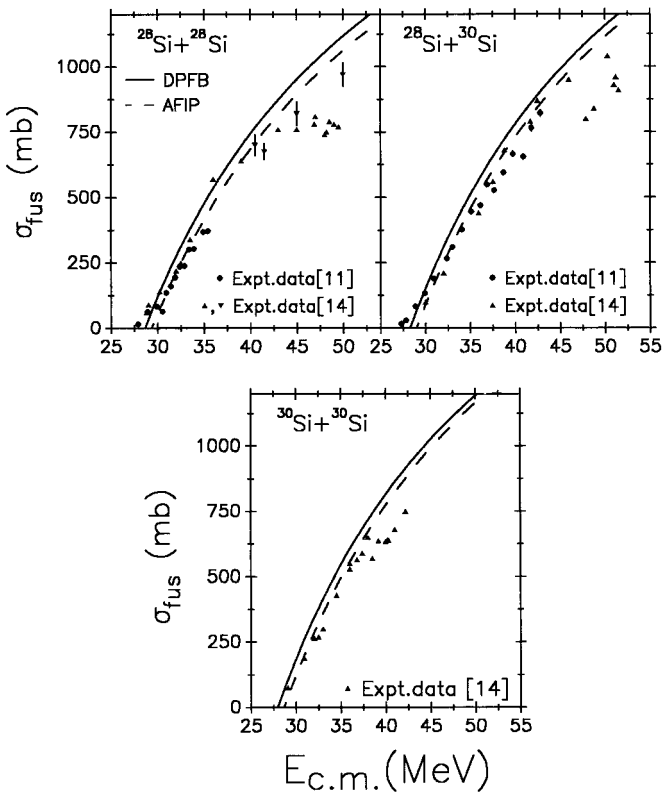

Fig. 12. Same as Fig. 11, but for $^{28}Si+^{28}Si$, $^{28}Si+^{30}Si$ and $^{30}Si+^{30}Si$ reactions

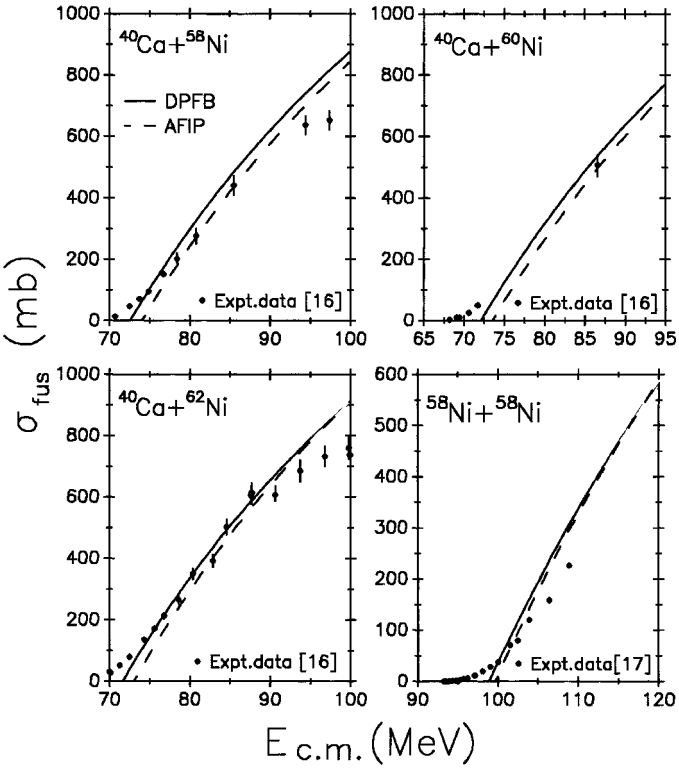

Fig. 14. Same as for Fig. 8, but for $^{40}Ca+^{58}Ni$, $^{40}Ca+^{60}Ni$, $^{40}Ca+^{62}Ni$ and $^{58}Ni+^{58}Ni$ reactions

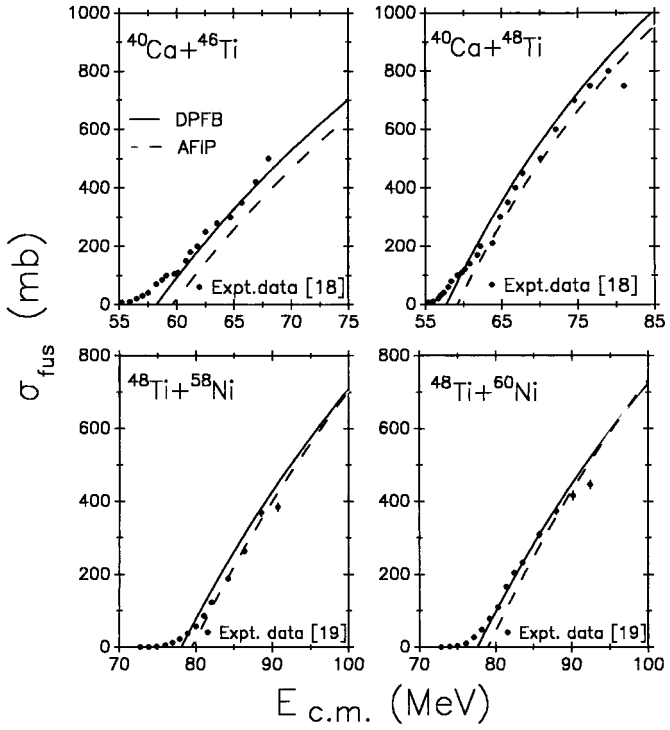

Fig. 15. Same as for Fig. 8, but for $^{40}Ca+^{46}Ti$, $^{40}Ca+^{48}Ti$, $^{48}Ti+^{58}Ni$ and $^{46}Ti+^{60}Ni$ reactions. The experimental data is from [18,19]

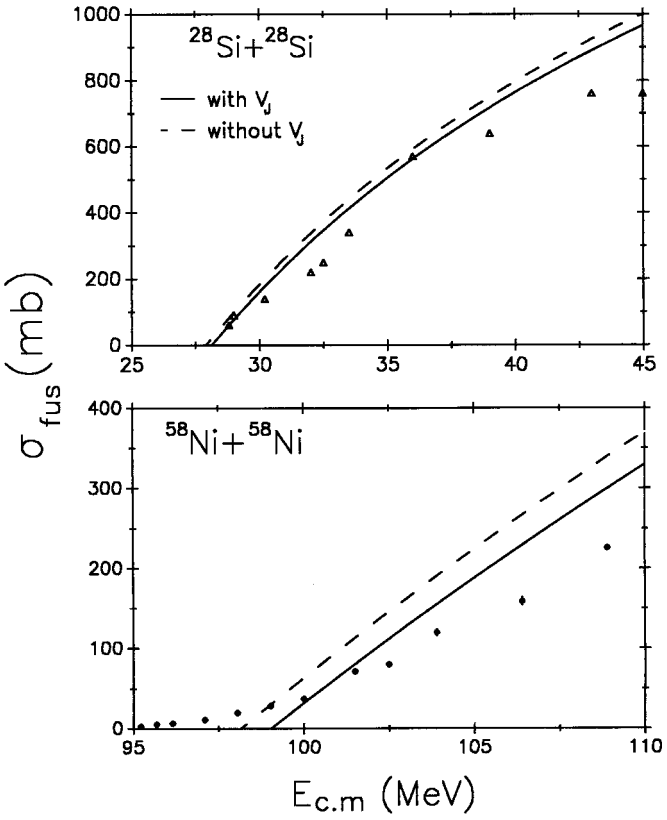

Fig. 16. The calculated fusion excitation functions for $^{28}Si+^{28}Si$ and $^{58}Ni+^{58}Ni$ reactions using the exact EDF, with and without spin-orbit density part included, compared with the experimental data

Finally, it would be of interest to see the contribution of spin-orbit density potential towards the fusion cross-section. In Fig. 16, we present the fusion excitation functions for the reactions of $^{28}Si+^{28}Si$ and $^{58}Ni+^{58}Ni$, using only the exact EDF. In one case, both spin-independent and spin-dependent parts are taken into account (dashed lines) whereas in the other case only spin-independent part is considered (solid lines). We find that the spin-orbit density term contributes quite appreciably towards fusion cross-sections. One should keep in mind that Si and Ni are highly spin-unsaturated nuclei. If one studies the collisions of spin-saturated or nearly saturated cases, then one may neglect the contribution of spin-density part.

In some of the fusion excitation functions discussed above, one may see some differences between the experimental data and theoretical calculations (AFIP or DPFB) at higher incident energies. This discrepency is due to the fact that here we use the sharp cut off model for fusion excitation functions. This model is valid for incident energies near and little above the fusion barrier. Therefore, we donot expect present calculations to reproduce the experimental excitation functions at higher incident energies. In order to study fusion at sub-barrier or at higher incident energies, more refine models, like the barrier penetration model, should be used.

From the above discussion, it is clear that the direct parameterization of fusion barriers or of ion-ion interaction potential yield nearly the same results which are in good agreement with most of the experimental data and the other theoretical results. Apparently, if one is interested in the fusion excitation functions only, the use of direct parameterization (DPFB) is straight forward since it depends only on the masses and charges of colliding nuclei. On the other hand, if one is also interested in studying other processes like elastic scattering, etc., which require the total ion-ion potential, one must use the analytical formula of interaction potential, the AFIP which gives the analytical formulation of ion-ion potential including the spin-orbit density part.

4 Summary

We have presented a detailed analysis of the fusion excitation functions, including a comparison with the available experimental data. The fusion excitation functions are calculated by using two different parameterizations. These parameterizations were based on Skyrme energy density formalism. In the first case, the ion-ion potential was parameterized and then, by adding Coulomb potential, one can compute the fusion barriers and excitation functions. In the second parameterization, the calculated fusion barrier heights and positions were parameterized directly. This detailed comparison gives us the possibility to test the accuracy and validity of these two available parameterizations.

We have calculated the fusion excitation functions for more than 50 reactions, ranging from $^{16}O + ^{16}O$ to $^{58}Ni + ^{58}Ni$. Due to the restriction in one of the analytical formulation, we calculated only those reactions where the target and projectile nuclei belong to the same shell. Our calculations clearly show that both parameterizations are able to reproduce the empirical data and the exact theoretical results quite nicely. Apart from this, our results are in good agreement with other theoretical calculations.

References

1. L.C. Vaz, J.M. Alexander and G.R. Satchler, Phys. Reports **69**, 373 (1981); M. Beckerman, Rep. Prog. Phys. **51**, 1047 (1988)
2. R.K. Puri and S. Kumar, Phys, Rev. **C57**, 2744(1998); S. Kumar and R.K. Puri, Phys. Rev. **C58**, 2858(1998); R.K. Puri, Ch. Hartnack and J. Aichelin, Phys. Rev. **C54**, R28 (1996); J. Aichelin, Phys. Reports. **202**, 233 (1991)
3. K.E. Zyromski et.al, Phys. Rev. **C55**, R562 (1997)
4. R.K. Puri, M.K. Sharma and R.K. Gupta, Eur. Phys. J. **A 3**, 277 (1998)
5. E.F. Aguilera, J.J. Kolata and R.J. Tighe, Phys. Rev. **C 52**, 3103 (1995); E.F. Aguilera, J.J. Vega, J.J. Kolata, A. Morsad, R.J. Tighe and X.J. Kong, Phys. Rev. **C 41**, 910 (1990)
6. D.G. Kovar, D.F. Geesaman, T.H. Braid, Y. Eisen, W. Henning, T.R. Ophel, M. Paul, K.E. Rehm, S.J. Sanders, P. Sperr, J.P. Schiffer, S.L. Tabor, S. Vigdo, B. Zeidman and F.W. Prosser Jr., Phys. Rev. **C 20**, 1305 (1979); and references therein
7. D. Shapira et. al., Phys. Rev. **C 28**, 1148 (1983)
8. S.L. Tabor, D.F. Geesaman, W. Henning, D.G. Kovar, K.E. Rehm and F.W. Prosser Jr., Phys. Rev. **C 17**, 2136 (1978)
9. R. Rascher, W.F.J. Muller and K.P. Lieb, Phys. Rev. **C 20**, 1028 (1979)
10. D.F. Geesaman, C.N. Davids, W. Henning, D.G. Kovar, K.E. Rehm, J.P. Schiffer, S.L. Tabor and F.W. Prosser Jr., Phys. Rev. **C 18**, 284 (1978)
11. S. Gary and C. Volant, Phys. Rev. **C 25**, 1877 (1982)
12. C.M. Jachcinski, D.G. Kovar, R.R. Betts, C.N. Davids, D.F. Geesaman, C. Olmer, M. Paul, S.J. Sanders and J.L. Yntema, Phys. Rev. **C 24**, 2070 (1981)
13. G.M. Berkowitz, P. Braun-Munzinger, J.S. Karp, R.H. Freifelder, T.R. Renner and H.W. Wilschut, Phys. Rev. **C 28**, 667 (1983); H.H. Gutbrod, W.G. Winn and M. Blann, Nucl. Phys. **A213**, 267 (1973)
14. E.F. Aguilera, J.J. Kolata, P.A. DeYoung and I.J. Vega, Phys. Rev. **C 33**, 1961 (1986); S.B. DiCenzo, J.F. Petersen and R.R. Betts, Phys. Rev. **C 23**, 2561 (1981)
15. E. Tomasi, D. Ardouin, J. Barreto, V. Bernard, B. Cauvin, C. Magnago, C. Mazur, C. Ngŏ, E. Piasecki and M. Ribarg, Nucl. Phys. **A373**, 341 (1982); H. Doubre et.al, Phys. Lett. **B 73**, 135 (1978); J. Barreto et.al, Phys. Rev. **C27**, 1335 (1983)
16. B. Sikora, J. Bisplinghoff, W. Scobel, M. Beckerman, M. Blann, Phys. Rev. **C 20**, 2219 (1979)
17. M. Beckerman et.al, Phys. Rev. **C 25**, 837 (1982)
18. A.A. Sonzogni, J. D. Bierman, M.P. Kelly, J.P. Lestone, J.F. Liang and R. Vandenbosch, Phys. Rev. **C 57**, 722 (1998)
19. A.M. Vinodkumar, K.M. Varier, N.V.S.V. Prasad, D.L. Sastry, A.K. Sinha, N. Madhavan, P. Sugathan, D.O. Kataria and J.J. Das, Phys. Rev. **C 53**, 803 (1996)
20. D.E. Di Gregorio et al., **C 39**, 516 (1989); P.R.S. Gomes et al., Phys. Rev. **C 49**, 245 (1994); P. Jacobs, Z. Frankel, G. Mamame, and I. Tserruya, Phys. Letts **B 175**, 271 (1986), S.Gil et al., Phys. Rev. Lett. **65**, 3100 (1990)
21. C. Ngŏ, B. Tamain, M. Breiner, R. J. Lombard, D. Mas, and H. H. Deubler, Nucl. Phys. **A 252**, 237 (1975); H. Ngŏ and Ch. Ngŏ, Nucl. Phys. **A 348**, 140 (1980)
22. K.C. Panda, and T. Patra, J. Phys. G: **14**, 1489 (1988)
23. D.M. Brink and N. Rowley, Nucl. Phys. **A 219**, 79 (1974); D.M. Brink and Fl. Stancu, Nucl. Phys. **A 243**, 175 (1975)
24. M. Brack et.al, Phys. Rep. **123**, 275 (1985)
25. G.Q. Li and G.Q. Xu, Nucl. Phys. **A492**, 340 (1989); G.Q. Li and G.Q. Xu, Phys. Rev. **C39**, 276 (1989)
26. H.J. Krappe, J.R. Nix, and A.J. Sierk, Phys. Rev. **C 20**, 992 (1979)
27. J. Blocki, J. Randrup, W.J. Swiatecki and C.F. Tsang, Ann. Phys. (NY) **105**, 427 (1977)
28. R.K. Puri, P. Chattopadhyay and R.K. Gupta, Phys. Rev. **C 43**, 315 (1991); R.K. Puri and R.K. Gupta, J. Phy. G. **17**, 1933 (1991); M.K. Sharma, H. Kumar, R.K. Puri and R.K. Gupta, Phys. Rev. **C 56**, 1175 (1997)
29. M.K. Sharma, R.K. Puri and R.K. Gupta, Z. Phys. **A 359**, 141 (1997)
30. R.K. Puri and R.K. Gupta, Phys. Rev. **C 45**, 1837 (1992)
31. R.K. Puri and R.K. Gupta, Int. Mod. Phys. **E1**, 269 (1992); M.K. Sharma, R.K. Puri and R.K. Gupta, Eur. Phys. J. **A2**, 69 (1998)
32. D. Vautherin and D. M. Brink, Phys. Rev. **C 5**, 626 (1972)
33. K.A. Bruckner, J.R. Buchler and M. Kelley, Phys. Rev. **173**, 944 (1968)
34. R. Arora, R.K. Puri and R.K. Gupta, Phys. Rev. C, in preperation